NANO LETTERS

pubs.acs.org/NanoLett Letter

Probing the Optical Response and Local Dielectric Function of an Unconventional Si@MoS_2 Core–Shell Architecture

Yea-Shine Lee, Sina Abedini Dereshgi, Shiqiang Hao, Matthew Cheng, Muhammad Arslan Shehzad, Christopher Wolverton, Koray Aydin, Roberto dos Reis, and Vinayak P. Dravid*

Cite This: *Nano Lett.* 2022, 22, 4848–4853 Read Online

ABSTRACT: Heterostructures of optical cavities and quantum emitters have been highlighted for enhanced light-matter interactions. A silicon nanosphere, *core*, and MoS_2, *shell*, structure is one such heterostructure referred to as the core@shell architecture. However, the complexity of the synthesis and inherent difficulties to locally probe this architecture have resulted in a lack of information about its localized features limiting its advances. Here, we utilize valence electron energy loss spectroscopy (VEELS) to extract spatially resolved dielectric functions of Si@MoS_2 with nanoscale spatial resolution corroborated with simulations. A hybrid electronic critical point is identified ~3.8 eV for Si@MoS_2. The dielectric functions at the Si/MoS_2 interface is further probed with a cross-sectioned core–shell to assess the contribution of each component. Various optical parameters can be defined via the dielectric function. Hence, the methodology and evolution of the dielectric function herein reported provide a platform for exploring other complex photonic nanostructures.

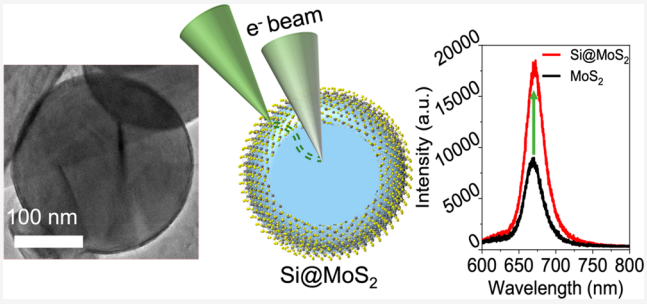

KEYWORDS: *core–shell architectures, two-dimensional materials, dielectric functions, optical resonators, Kramers–Kronig analysis*

Semiconductor transition metal dichalcogenides (TMDs) of the formula MX_2 (M = transition metal; X = chalcogen) in the two-dimensional materials family have earned significant interest in the past decade. One outstanding feature of TMDs is their large exciton binding energy and exciton transition dipole moment, making them strong candidates as quantum emitters for next-generation photonics even at room temperature.[1] Reports have been made on improving the functionality of the TMDs by encapsulating a nanosphere core material, such as Au,[2,3] Ag,[3,4] and Si.[5,6] In such core–shell architectures, light–matter interactions are enhanced by the surface interaction between the core and the shell.[1] This is promising for optoelectronic applications such as exciton–polariton lasers, light-emitting devices, and all-optical switches.[7] For example, plasmonic core materials such as Au and Ag that have been encapsulated with TMDs are reported to show improved TMD photoluminescence (PL) intensity.[8−10] However, plasmonic core materials are prone to Ohmic losses,[11] which has led to replacing these cores with high refractive index dielectric materials such as Si.[5] Electric field penetrates dielectric materials, unlike their metallic counterparts. Therefore, dielectric materials with a high refractive index can support multiple optical modes, which offer tunable energy coupling upon overlap with the exciton transition of the TMD.

With rising interests in these hybrid core–shell architectures for photonic applications, it has become increasingly important to understand the precise structure–property relationship of this system. In this work, we begin with a macroscale observation of the aforementioned improved light–matter interaction in Si@MoS_2 in the form of enhanced PL relative to planar MoS_2. We then evaluate the dielectric function at different localized parts of the core–shell architecture in the nanoscale. In a dielectric function, $\varepsilon = \varepsilon_1 + i\varepsilon_2$, the real part ($\varepsilon_1$) underscores the material's ability to store electrical energy (electronic polarizability) and its refractive index while the imaginary part (ε_2) incorporates the material's energy loss or light absorption.[12] By conducting a comparative study on the core–shells against the unencapsulated Si nanosphere and planar MoS_2, we probe how both the electronic structure and optical properties can be tuned in complex hybrid architectures. The extended connection to macroscopic properties, such as PL, will ultimately assist to improve property–performance relationships.

To study the dielectric functions of this system, valence electron energy loss spectroscopy (VEELS) is adopted. VEELS yields high spatial resolution in the nanometer scale, which enables an investigation of localized features. The low energy

Received: March 25, 2022
Revised: June 6, 2022
Published: June 8, 2022

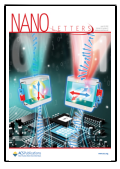

https://doi.org/10.1021/acs.nanolett.2c01221
Nano Lett. 2022, 22, 4848–4853

loss region captures electronic structure information such as valence electron excitation, plasmonic excitations, and intra/interband transitions based on the band structure, which govern the optical properties of a material.[13] Therefore, VEELS can be used to extract the complete complex dielectric function, which can unlock information on optical properties, such as absorption coefficient, reflectance, and transmissivity using the Kramers−Kronig analysis (KKA).[14,15]

The silicon nanospheres we use range from 100 to 200 nm in diameter, and the MoS_2 shell encapsulating the nanosphere ranges between 5- and 15-layers, where each layer is ∼0.63 nm thick (see Figure S1).[16] The encapsulation is achieved via chemical vapor deposition (CVD). The spherical core−shell architecture is expected to have an increased PL intensity as the electric field in the near-field region around the core is enhanced and the light interaction with MoS_2 is improved.[3,8] A magnetic dipole (MD) mode is formed inside the Si core and the electric field is concentrated outside the core (MoS_2 shell region) region. The MD mode is coupled to the exciton modes of MoS_2. Hence, this system effectively acts as a cavity and enhances PL (see Figure S2). This enhancement is observed in a 23 × 10 μm^2 scan of a region on the Si@MoS_2 growth substrate as shown in the optical image of Figure 1a. The growth substrate is a Si/SiO_2 (300 nm thick oxide layer) wafer, on which clusters of Si nanoparticles are dispersed and MoS_2 is grown throughout the substrate. Therefore, the growth substrate has Si@MoS_2 as well as planar MoS_2 on regions where there are no nanoparticles. This enables PL intensity comparison of planar MoS_2 and Si@MoS_2 under identical parameters, eliminating possible errors from differing CVD growth conditions.

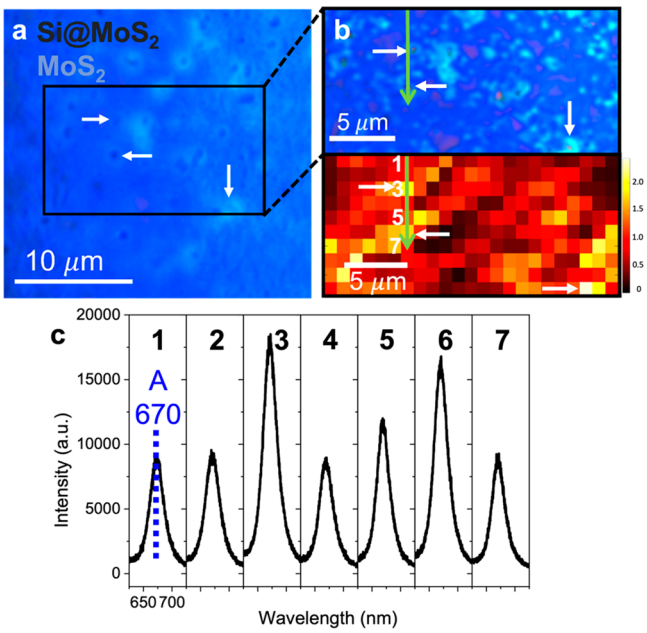

Figure 1. (a) Out-of-focus optical image of growth substrate at 150× magnification (100× objective followed by 1.5× ocular) depicting clusters of Si@MoS_2 in black spherical specks. The region of interest for PL mapping is boxed. (b) In-focus optical image at 150× magnification of a Si@MoS_2 growth substrate. The dimensions are 23 × 10 μm^2, and a few Si@MoS_2 clusters are marked with white arrows. Corresponding PL map of the same region of interest below. Each pixel is 1 μm scale. (c) Representative PL spectra down the line profile in green arrow marked in panel b.

Figure 1a is an out-of-focus optical image of the growth substrate at 150× magnification on which Si@MoS_2 clusters appear as black specks. Figure 1b is an in-focus optical image of the region of interest for PL mapping. Clusters of Si nanoparticles are marked in white arrows to guide the eye. Also presented is the PL map of the same region. Brighter colors correspond to higher PL intensity at 670 nm, the expected A-exciton peak for MoS_2.[17−19] From Figure 1c, the representative PL spectra extracted along the line profile, it is evident that Si@MoS_2 clusters yield higher PL intensity than the adjacent regions of planar MoS_2.

This macroscopic photonic phenomenon suggests a transformation not only at the micron scale but also at the nanoscale as the silicon and MoS_2 are superposed in a core−shell geometry. Therefore, VEELS is employed as a technique to investigate the system with high spatial resolution and acceptable energy resolution. As can be seen from the full width at half-maximum (fwhm) of the zero-loss peak (ZLP) in Figure S3, the energy resolution of our spectroscopy system is approximately 0.6 eV. As the tail of the ZLP is overlapped with the peaks corresponding to the band gaps of Si and MoS_2, further discussion focuses on peaks beyond the band gap energy range.

As an experimental control, planar MoS_2 flakes and unencapsulated Si nanoparticles are separately transferred from the growth substrate to lacey carbon Cu transmission electron microscope (TEM) grids. Scanning TEM (STEM) annular dark-field (ADF) images are shown in Figure 2a and b for MoS_2 and Si nanoparticles, respectively. VEELS is used to corroborate the robustness of the chemical composition after the transfer process. As shown in Figure S4, the spectra show a Si plasmon peak at 16.7 eV, in good agreement with the literature value.[20] The plasmon peaks of MoS_2 appear at 8 eV (π plasmon) as a small bump attributed to six π-electrons four of which are attributed to the sulfur at the van der Waals layer, and at 23 eV ($\pi + \sigma$ plasmon), from the collective oscillations of all valence electrons. Both experimental peaks are again in good agreement with what is reported in literature,[21,22] although hydrocarbon contamination during spectra acquisition also contributes to the peak at 23 eV.

From these VEELS spectra, the dielectric functions are extracted as shown in Figure 2b and e (refer to the Supporting Information for details). Although the precision of the spectra gives confidence in the dielectric function extractions, it is expected that experimental artifacts occur upon performing KKA. For example, the surface contamination of hydrocarbons or oxidation, as well as interactions from Cherenkov radiation or surfaces losses may be present.[14,23] Defects in the structure, such as incomplete encapsulation, line defects and strain, can also alter ε_2 from band gap changing.[13] Defined in units of local inelastic mean free path of electrons, sample thickness effects may also carry over in KKA if the value is significantly larger than 1. Calculated by sample thickness over inelastic mean free path (t/λ), this value is extracted using the relative log-ratio method. For the silicon nanosphere and planar MoS_2 in Figure 2, these are 1.38 and 0.65, respectively. Hence, thickness effects in the nanosphere can contribute to peak broadening in addition to the energy resolution as in Figure 2e. Therefore, simulations are conducted (described in Supporting Information) to more robustly compare against potential experimental artifact features. The results are shown in Figure

https://doi.org/10.1021/acs.nanolett.2c01221
Nano Lett. 2022, 22, 4848−4853

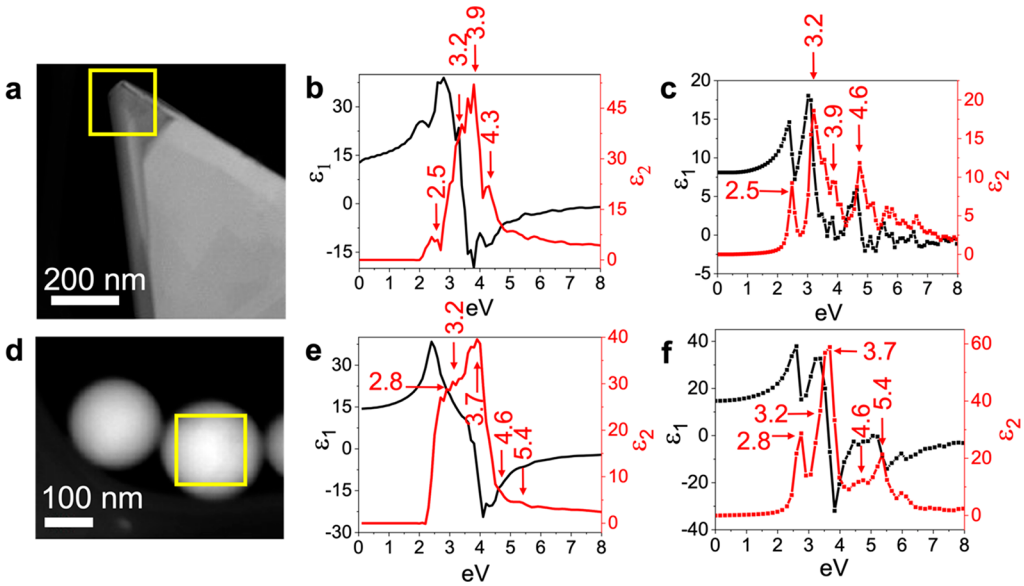

Figure 2. (a) STEM-ADF image of planar MoS_2. (b) Experimental dielectric function of planar MoS_2 flake extracted from the region boxed in panel a. (c) Simulated dielectric function of a monolayer MoS_2. (d) STEM-ADF image of unencapsulated Si nanospheres. (e) Experimental dielectric function of the unencapsulated Si nanoparticle extracted from the region boxed in panel d. (f) Simulated dielectric function of bulk Si. The exchange-correlation energy is calculated within the G0W0 approximation in simulations (see Supporting Information for details).

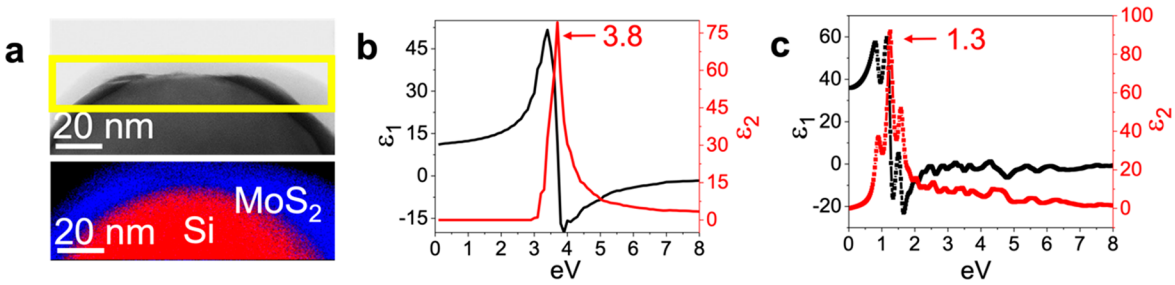

Figure 3. (a) STEM-ADF image of a core−shell with an elemental map corresponding to the boxed region. (b) Dielectric function of the boxed region in (a). c) Simulated dielectric function of monolayer MoS_2-bulk Si planar heterostructure. The exchange-correlation energy is calculated within the G0W0 approximation in the simulation (see Supporting Information for details).

2c and f. Simulations of dielectric functions of MoS_2 assume a planar monolayer measured in the *xy*-orientation, while that of Si assumes a planar bulk structure.

Peaks in ε_2 indicate critical points in the electronic transitions, representative of the nature of the material, and both simulations are in good agreement with the experimental dielectric functions. The prominent peaks in MoS_2 ε_2 appear ∼2.5, 3.2, and 3.9 eV, with broader peaks trailing at energies greater than 4.3 eV. The parallel lowest conduction band and highest valence band between the M and Γ points in the Brillouin zone yields a strong optical critical point ∼2.5 eV.[24−26] The next peak ∼3.0 eV is attributed to the electron−hole pairs at the transition between the K and Γ Brillouin zones, where the conduction and valence band minima are parallel.[24,27] The parallel bands yield maximum joint density of states. Above this is the critical point ∼3.9 eV, whose origin is uncertain and seldom reported in literature. Considering the sizable energy, it likely corresponds to a combination of multiple higher critical points as do higher energy peaks, which is common for semiconductors.[24,26]

The prominent peaks in the Si ε_2 function appear ∼2.8, 3.2, and 3.7 eV with smaller, broader peaks ∼4.6, and 5.4 eV. The peak ∼2.8 eV is attributed to the silicon direct band gap, while the rest are attributed to higher transitions.[28] The peak ∼3.2 eV aligns with the $\Gamma_{25'} \rightarrow \Gamma_{15}$ transition, while the peak ∼3.7 eV aligns with $L_{3'} \rightarrow L_1$ transition in the silicon band structure. Higher energy peaks ∼4.6 and 5.4 eV correspond to $X_4 \rightarrow X_1$ and $L_{3'} \rightarrow L_3$ transitions, respectively (Figure S5).[28,29]

Next, Si@MoS_2 are transferred to TEM grids in a similar manner. The STEM-ADF image of a core−shell is shown in Figure 3a. The compositional integrity is confirmed by the chemical composition map derived using a least-squares function to fit Lorentzian curves to VEELS Si and MoS_2 peaks as shown in Figure S6. The dielectric function of the core−shell architecture is extracted where t/λ is 0.75 as shown in Figure 3b. The dielectric function of the core−shell is similar to those of the individual core and shell components at first glance. However, there are fewer dispersed peaks overall, and one narrow peak ∼3.8 eV in ε_2 is prominent. This peak is possibly from a critical point in the hybridized electronic structure of the core−shell. The narrow width of this peak also suggests that other critical transitions identified in the individual Si and MoS_2 components are relatively suppressed. Spatial redistribution of charge carriers and modifications in their interactions upon heterostructuring semiconductors with different band gaps is a well-known phenomenon that justifies this transformation.[30]

https://doi.org/10.1021/acs.nanolett.2c01221
Nano Lett. 2022, 22, 4848−4853

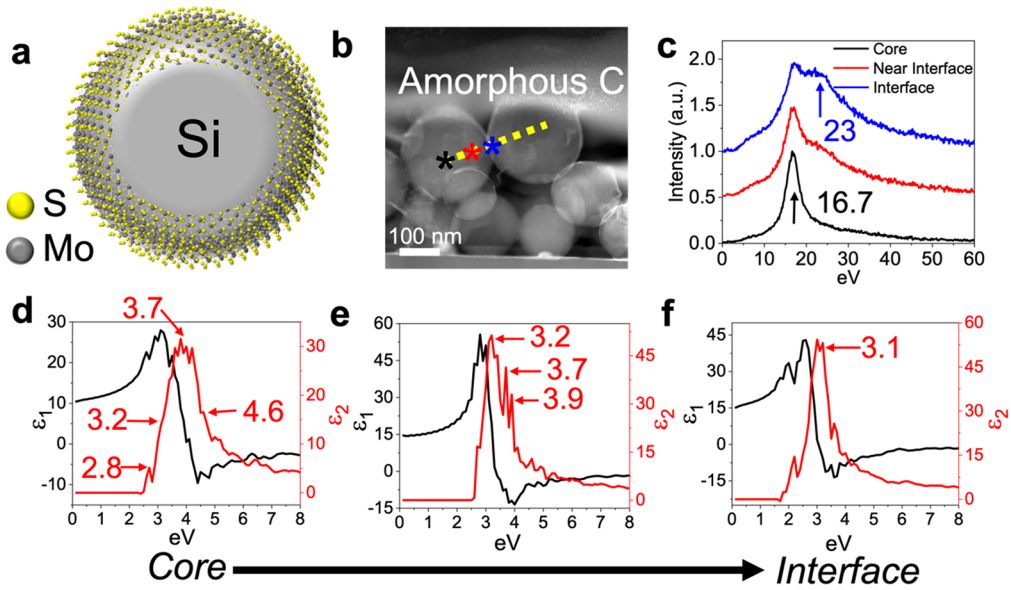

Figure 4. (a) Schematic of a cross-sectional core−shell. (b) STEM-ADF image of a cross-sectional sample capturing multiple Si@MoS_2 on Si/SiO_2 growth substrate and covered by an amorphous carbon capping layer. (c) VEELS spectra extracted along a line profile at the Si core, near the core−shell interface, and at the core−shell interface as marked with corresponding colored stars in panel b. Curves are offset by 0.5 units. (d) Dielectric function extracted at the core (black star), (e) near the core−shell interface (red star), and (f) core−shell interface (blue star) along the line profile in panel b.

A planar heterostructure of two atomic layers thick Si and monolayer MoS_2 is adopted in the core−shell simulation due to several challenges with accurately representing the experimental model. These challenges include (1) the diameter of the core−shell spanning hundreds of nanometers, (2) uncertainty regarding lattice mismatch and surface reconstruction at the silicon−MoS_2 interface, (3) defects in the MoS_2, such as buckling, and (4) curvature of the core resulting in lattice strain build up. All of these factors will alter the band gap relative to experimental conditions contributing to the ∼2.5 eV red-shift of the simulated dielectric function from experimental results as shown in Figure 3c.

Moreover, the band gap of the calculated heterostructure of Si−MoS_2 is rather small (0.15 eV), which is much smaller than the 5-layer MoS_2 (1.4 eV), contributing to the red-shift of the calculated spectrum. The small band gap is due to the hybridization of Si 3p state and Mo 4d state as shown in the density of states lowest peak in the conduction band (Figure S5). Unlike band structure calculations of the individual components core and shell, that of the spherical core−shell heterostructure is hence much more sophisticated. This upholds the importance of experimentally acquiring the dielectric function to provide a survey of the electronic structure of complex geometries. VEELS is a powerful technique to assist such information acquisition with nanoscale spatial resolution.

Investigation of a cross-sectional core−shell is seldom reported because of the long-standing difficulties involved in slicing a nanosized sphere. Here, we present a cross-sectional sample prepared by focused ion beam (FIB) as shown in the schematic and STEM-ADF image in Figure 4a and b, offering insights distinct from the traditional holistic analysis of this nanostructure. Moreover, the cross-sectional sample retains the clustered nature of core−shells on the growth substrate, replicating factors that better resemble application conditions of these systems.

VEELS spectra taken at three different points along a line profile in the cross-sectional sample is shown in Figure 4c. The line crosses the shaved core of Si@MoS_2 to the intact core−shell interface, enabling a localized study of the system at each pixel corresponding to 2 nm. The deconvoluted spectra are shown for clarity in Figure S7. The expected Si plasmon peak dominates at the core at 16.7 eV.[20] The MoS_2 peak is absent at the core, ensuring the removal of the shell slice in the cross-section. The MoS_2 plasmon peak intensifies closer to the edge of the system, at the expected energy of 23 eV, where the shell structure is still intact.[21,22] As the spectra at the three points are in agreement with literature values, we have confidence in extracting the dielectric functions at these points.

To gain further insights into the transformations induced upon forming the heterostructure, the dielectric function is also extracted from the three different features of the core−shell architecture: the core, near the interface, and at the core−shell interface (Figure 4d−f). The increased noise in the functions is due to a smaller pixel area coverage in the line profile. As expected, the dielectric function at the core in Figure 4d aligns well with that of the unencapsulated Si nanoparticle (Figure 2f) in terms of peak energies. Moving toward the core−shell interface in Figure 4f, the peak width in ε_2 narrows and there is a greater overlap between ε_1 and ε_2, resembling the dielectric function of holistic Si@MoS_2 (Figure 3b), particularly the peak ∼3.1 eV. A significant contribution from the dielectric function of MoS_2 is also observed since the interface has a relatively greater contribution from the MoS_2 shell than does the holistic coverage of Si@MoS_2. The dielectric function at the interface can also be treated as a slight red-shift from that of the planar MoS_2 flake, which may be caused by curvature strain induced band shifting.[31]

In conclusion, while the sufficient coverage of the core−shell architecture in Figure 3 gives the monolithic electronic structure from its dielectric function, regions along the line profile can give more localized information with higher spatial accuracy. The merit of VEELS is that the electronic structure

https://doi.org/10.1021/acs.nanolett.2c01221
Nano Lett. 2022, 22, 4848−4853

transformation can be directly isolated and traced along local features of the heterostructure in this manner. Further work with improved energy resolution may better reveal finer states such as vibrational low energy states. However, the main challenge is that responses from complex heterostructures are inherently difficult to deconvolve into contributions from each component. This study presents the first steps to isolating features of complex heterostructures to probe the localized dielectric function by nanoscale sample preparation and experimental methods, namely cross-sectioning and VEELS. Our work opens avenues to explore regions of a complex geometry, including potential defects, with high spatial resolution for optimized performance of a specific material property. Therefore, the ability to investigate the core−shell architectures, an excellent next generation photonic device, utilizing spectroscopic information in this manner lays the ground for work in other advanced optical nanomaterials.

■ ASSOCIATED CONTENT

Supporting Information

The Supporting Information is available free of charge at https://pubs.acs.org/doi/10.1021/acs.nanolett.2c01221.

Experimental methods, CVD synthesis protocol and chemical mapping of Si@MoS_2, electric field enhancement in the core near-field, zero-loss peak of EELS spectra, energy loss functions and band structure calculations of Si and MoS_2 and Si@MoS_2, deconvoluted VEELS spectra of cross sectional Si@MoS_2 clusters, and calculated dielectric functions of 5-layer planar MoS_2 with different energy resolution parameters (PDF)

■ AUTHOR INFORMATION

Corresponding Author

Vinayak P. Dravid − *Department of Material Science and Engineering, Northwestern University Atomic and Nanoscale Characterization Experimental (NUANCE) Center, and International Institute for Nanotechnology (IIN), Northwestern University, Evanston, Illinois 60208, United States;* orcid.org/0000-0002-6007-3063; Email: v-dravid@northwestern.edu

Authors

Yea-Shine Lee − *Department of Material Science and Engineering, Northwestern University, Evanston, Illinois 60208, United States;* orcid.org/0000-0002-2087-4886

Sina Abedini Dereshgi − *Department of Electrical and Computer Engineering, Northwestern University, Evanston, Illinois 60208, United States;* orcid.org/0000-0003-2929-0817

Shiqiang Hao − *Department of Material Science and Engineering, Northwestern University, Evanston, Illinois 60208, United States;* orcid.org/0000-0002-7985-4468

Matthew Cheng − *Department of Material Science and Engineering, Northwestern University, Evanston, Illinois 60208, United States;* orcid.org/0000-0002-1062-5974

Muhammad Arslan Shehzad − *Department of Material Science and Engineering and Northwestern University Atomic and Nanoscale Characterization Experimental (NUANCE) Center, Northwestern University, Evanston, Illinois 60208, United States;* orcid.org/0000-0002-6260-5764

Christopher Wolverton − *Department of Material Science and Engineering, Northwestern University, Evanston, Illinois 60208, United States;* orcid.org/0000-0003-2248-474X

Koray Aydin − *Department of Electrical and Computer Engineering, Northwestern University, Evanston, Illinois 60208, United States;* orcid.org/0000-0002-3268-2216

Roberto dos Reis − *Department of Material Science and Engineering, Northwestern University Atomic and Nanoscale Characterization Experimental (NUANCE) Center, and International Institute for Nanotechnology (IIN), Northwestern University, Evanston, Illinois 60208, United States*

Complete contact information is available at: https://pubs.acs.org/10.1021/acs.nanolett.2c01221

Author Contributions

The manuscript was written through contributions of all authors. All authors have given approval to the final version of the manuscript.

Notes

The authors declare no competing financial interest.

The data that support the findings of this study are available from the corresponding author upon reasonable request.

■ ACKNOWLEDGMENTS

This work was supported by NSF Division of Material Research (NSF Grant DMR-1929356—Program Manager: Lynnette Madsen). This work made use of the EPIC facility of Northwestern University's NUANCE Center, which has received support from the SHyNE Resource [National Science Foundation (NSF) Grant ECCS-2025633], Northwestern's MRSEC program (NSF Grant DMR-1720139), the Keck Foundation, and the State of Illinois through IIN. The materials synthesis in this work was partially supported by the Army Research Office (Grant W911NF1910335). K.A. acknowledges support from the Office of Naval Research Young Investigator Program (ONR-YIP) Award (N00014-17-1-2425). The authors wish to thank Dr. Tatsuki Hinamoto, Dr. Hiroshi Sugimoto, and Dr. Minoru Fujii from Kobe University for providing the silicon nanospheres.

■ REFERENCES

(1) Baranov, D. G.; Wersäll, M.; Cuadra, J.; Antosiewicz, T. J.; Shegai, T. Novel Nanostructures and Materials for Strong Light−Matter Interactions. *ACS Photonics* **2018**, *5* (1), 24−42.

(2) DiStefano, J. G.; Murthy, A. A.; Lescott, C. J.; dos Reis, R.; Li, Y.; Dravid, V. P. Au@MoS2@WS2 Core−Shell Architectures: Combining Vapor Phase and Solution-Based Approaches. *J. Phys. Chem. C* **2020**, *124* (4), 2627−2633.

(3) Lepeshov, S.; Wang, M.; Krasnok, A.; Kotov, O.; Zhang, T.; Liu, H.; Jiang, T.; Korgel, B.; Terrones, M.; Zheng, Y.; Alú, A. Tunable Resonance Coupling in Single Si Nanoparticle−Monolayer WS2 Structures. *ACS Appl. Mater. Interfaces* **2018**, *10* (8), 16690−16697.

(4) Kuznetsov, A. I.; Miroshnichenko, A. E.; Brongersma, M. L.; Kivshar, Y. S.; Luk'yanchuk, B. Optically Resonant Dielectric Nanostructures. *Science* **2016**, *354* (6314), aag2472.

(5) van de Haar, M. A.; van de Groep, J.; Brenny, B. J.M.; Polman, A. Controlling Magnetic and Electric Dipole Modes in Hollow Silicon Nanocylinders. *Opt. Express* **2016**, *24* (3), 2047−2064.

(6) Stamatopoulou, P. E.; Tserkezis, C. Role of Emitter Position and Orientation on Silicon Nanoparticle-Enhanced Fluorescence. *OSA Contin.* **2021**, *4* (3), 918−932.

(7) Wang, H.; Wen, J.; Wang, W.; Xu, N.; Liu, P.; Yan, J.; Chen, H.; Deng, S. Resonance Coupling in Heterostructures Composed of

Silicon Nanosphere and Monolayer WS2: A Magnetic-Dipole-Mediated Energy Transfer Process. *ACS Nano* **2019**, *13* (2), 1739−1750.
(8) Wu, Z.-Q.; Yang, J.-L.; Manjunath, N. K.; Zhang, Y.-J.; Feng, S.-R.; Lu, Y.-H.; Wu, J.-H.; Zhao, W.-W.; Qiu, C.-Y.; Li, J.-F.; Lin, S.-S. Gap-Mode Surface-Plasmon-Enhanced Photoluminescence and Photoresponse of MoS2. *Adv. Mater.* **2018**, *30* (27), 1706527.
(9) Yan, J.; Liu, X.; Mao, B.; Yang, G.; Li, B. Individual Si Nanospheres Wrapped in a Suspended Monolayer WS2 for Electromechanically Controlled Mie-Type Nanopixels. *Adv. Opt. Mater.* **2021**, *9* (5), 2001954.
(10) Butun, S.; Tongay, S.; Aydin, K. Enhanced Light Emission from Large-Area Monolayer MoS2 Using Plasmonic Nanodisc Arrays. *Nano Lett.* **2015**, *15* (4), 2700−2704.
(11) Cai, K.; He, C.; Xiao, F.; Rukhlenko, I. D.; Zhu, W. Resonant Mode Coupling in Hybrid All-Dielectric Metamaterial. *Mater. Res. Express* **2019**, *6* (12), 125801.
(12) Khan, W.; Betzler, S. B.; Šipr, O.; Ciston, J.; Blaha, P.; Scheu, C.; Minar, J. Theoretical and Experimental Study on the Optoelectronic Properties of Nb3O7 (OH) and Nb2O5 Photoelectrodes. *J. Phys. Chem. C* **2016**, *120* (41), 23329−23338.
(13) Brockt, G.; Lakner, H. Nanoscale EELS Analysis of Dielectric Function and Bandgap Properties in GaN and Related Materials. *Micron* **2000**, *31* (4), 435−440.
(14) Stöger-Pollach, M.; Laister, A.; Schattschneider, P. Treating Retardation Effects in Valence EELS Spectra for Kramers−Kronig Analysis. *Ultramicroscopy* **2008**, *108* (5), 439−444.
(15) Egerton, R. F. *Electron Energy-Loss Spectroscopy in the Electron Microscope*; Springer, 2011.
(16) Zhang, H.; Ma, Y.; Wan, Y.; Rong, X.; Xie, Z.; Wang, W.; Dai, L. Measuring the Refractive Index of Highly Crystalline Monolayer MoS2 with High Confidence. *Sci. Rep.* **2015**, *5* (1), 8440.
(17) Splendiani, A.; Sun, L.; Zhang, Y.; Li, T.; Kim, J.; Chim, C.-Y.; Galli, G.; Wang, F. Emerging Photoluminescence in Monolayer MoS2. *Nano Lett.* **2010**, *10* (4), 1271−1275.
(18) Li, H.; Zhu, X.; Tang, Z. K.; Zhang, X. H. Low-Temperature Photoluminescence Emission of Monolayer MoS2 on Diverse Substrates Grown by CVD. *J. Lumin.* **2018**, *199*, 210−215.
(19) Nan, H.; Wang, Z.; Wang, W.; Liang, Z.; Lu, Y.; Chen, Q.; He, D.; Tan, P.; Miao, F.; Wang, X.; Wang, J.; Ni, Z. Strong Photoluminescence Enhancement of MoS2 through Defect Engineering and Oxygen Bonding. *ACS Nano* **2014**, *8* (6), 5738−5745.
(20) Kissinger, G.; Kot, D.; Klingsporn, M.; Schubert, M. A.; Sattler, A.; Müller, T. Investigation of the Copper Gettering Mechanism of Oxide Precipitates in Silicon. *ECS J. Solid State Sci. Technol.* **2015**, *4* (9), N124.
(21) Moynihan, E.; Rost, S.; O'connell, E.; Ramasse, Q.; Friedrich, C.; Bangert, U. Plasmons in MoS2 Studied via Experimental and Theoretical Correlation of Energy Loss Spectra. *J. Microsc.* **2020**, *279* (3), 256−264.
(22) Disko, M. M.; Treacy, M. M. J.; Rice, S. B.; Chianelli, R. R.; Gland, J. A.; Halbert, T. R.; Ruppert, A. F. Spatially Resolved Electron Energy-Loss Spectroscopy of MoS2 Platelets. *Ultramicroscopy* **1987**, *23* (3), 313−319.
(23) Daniels, J.; Festenberg, C. v.; Raether, H.; Zeppenfeld, K. Optical Constants of Solids by Electron Spectroscopy. In *Springer Tracts in Modern Physics*, Vol. *54*; Höhler, G., Ed.; Springer: Berlin, 1970; pp 77−135. DOI: 10.1007/BFb0045980.
(24) Li, W.; Birdwell, A. G.; Amani, M.; Burke, R. A.; Ling, X.; Lee, Y.-H.; Liang, X.; Peng, L.; Richter, C. A.; Kong, J.; Gundlach, D. J.; Nguyen, N. V. Broadband Optical Properties of Large-Area Monolayer CVD Molybdenum Disulfide. *Phys. Rev. B* **2014**, *90* (19), 195434.
(25) Wang, H.; Yu, L.; Lee, Y.-H.; Shi, Y.; Hsu, A.; Chin, M. L.; Li, L.-J.; Dubey, M.; Kong, J.; Palacios, T. Integrated Circuits Based on Bilayer MoS2 Transistors. *Nano Lett.* **2012**, *12* (9), 4674−4680.
(26) Aspnes, D. E. Approximate Solution of Ellipsometric Equations for Optically Biaxial Crystals. *JOSA* **1980**, *70* (10), 1275−1277.
(27) Molina-Sánchez, A.; Sangalli, D.; Hummer, K.; Marini, A.; Wirtz, L. Effect of Spin-Orbit Interaction on the Optical Spectra of Single-Layer, Double-Layer, and Bulk MoS 2. *Phys. Rev. B* **2013**, *88* (4), 045412.
(28) Djemia, P.; Bouamama, K. Ab-Initiocalculations of the Photoelastic Constants of the Cubic SiC Polytype. *J. Phys. Conf. Ser.* **2013**, *454*, 012060.
(29) Welkowsky, M.; Braunstein, R. Interband Transitions and Exciton Effects in Semiconductors. *Phys. Rev. B* **1972**, *5* (2), 497−509.
(30) Kapuria, N.; Patil, N. N.; Ryan, K. M.; Singh, S. Two-Dimensional Copper Based Colloidal Nanocrystals: Synthesis and Applications. *Nanoscale* **2022**, *14* (8), 2885−2914.
(31) DiStefano, J. G.; Murthy, A. A.; Jung, H. J.; dos Reis, R.; Dravid, V. P. Structural Defects in Transition Metal Dichalcogenide Core-Shell Architectures. *Appl. Phys. Lett.* **2021**, *118* (22), 223103.

https://doi.org/10.1021/acs.nanolett.2c01221
Nano Lett. 2022, 22, 4848−4853